Available online at www.sciencedirect.com
ScienceDirect
Journal of Power Sources 159 (2006) 905–913
JOURNAL OF POWER SOURCES
www.elsevier.com/locate/jpowsour

Model based PEM fuel cell state-of-health monitoring via ac impedance measurements

N. Fouquet [a,b,*], C. Doulet [a,b], C. Nouillant [a], G. Dauphin-Tanguy [b], B. Ould-Bouamama [b]

[a] *PSA Peugeot-Citroën, Centre Technique de Vélizy, 2, Route de Gisy, Bat. 91 VV141, 78943 Vélizy-Villacoublay, France*
[b] *LAGIS UMR CNRS 8146, École Centrale de Lille, 59651 Villeneuve d'Ascq, France*

Received 11 September 2005; received in revised form 17 October 2005; accepted 9 November 2005
Available online 15 December 2005

Abstract

The present paper deals with monitoring of flooding and drying out of a proton exchange membrane (PEM) fuel cell using a model-based approach coupled with ac impedance measurements. A study of the impedance response of a 150 cm^2 six-cell air/H_2 PEM fuel cell as a function of inlet gas relative humidity was carried out. Parameters of a Randles-like equivalent circuit were then fitted to the data. In order to improve the quality of the fit, the classical Randles cell was extended by changing the standard plane capacitor into a constant phase element (CPE). It was found that monitoring the evolution of the three resistances of this modified Randles model was an efficient and robust way of monitoring the state-of-health (SOH) of the fuel cell with respect to the water content of the membrane electrode assembly. Moreover, the non-integer power of the CPE was found to be statistically constant over a wide range of operating conditions, thus comforting the assumption that it has a physical meaning. Qualitative interpretation of the variation of the parameters as a function of the SOH is proposed in both flooded and dry conditions.

Keywords: PEM fuel cell; Water management; Electrochemical impedance spectroscopy; Model-based fault detection and isolation

1. Introduction

1.1. Motivation and background

From an automotive manufacturer point of view, fuel cells have evolved, over the past decade, from a laboratory experiment to one of the most probable successors to the internal combustion engine. Now that vehicle integration has been demonstrated and performances are ramping up, command and control issues as well as fault detection and isolation (FDI) gather more importance to the day.

One of the major challenges in proton exchange membrane fuel cell FDI and control reconfiguration lies in the state of hydration of the membrane electrode assembly [1]. In a PEM fuel cell, the electrolyte is a polymer membrane that ensures proton conductivity between anode and cathode while being electronically insulated. Protons are able to cross the membrane only if attached to water molecules. Thus, it is of prime importance to ensure at all time a steady minimum water content in the electrolyte. To do so, water vapor is usually added to the feed stream, which can be quite a tricky task to achieve properly, for the following reasons:

- relative humidity sensors only measure the inlet/outlet water content of the gases, which are not straightforwardly linked to the state of hydration of the membrane electrode assembly, as we shall see later in this article,
- actuators, among which we can cite enthalpy wheels, gas/gas or water/gas membrane humidificator are often slow and/or inaccurate.

These technical shortcomings can lead to too much or too few water being injected in the fuel cell, which in turn causes flooding or drying out. Prolonged operation in either of these two states can be very harmful, or even fatal, to the stack [2].

The challenge of monitoring water distribution within a PEM fuel cell has been taken up by many research teams around the world over the past couple of years. Good results were obtained by using transparent bipolar plates [3], gas chromatography [4], or even neutron imaging [5]. However efficient they might be, it is very unlikely that these methods will ever find their way into mass production.

* Corresponding author. Tel.: +33 0157591551; fax: +33 0157593066.
E-mail address: nicolas.fouquet@mpsa.com (N. Fouquet).

0378-7753/$ – see front matter © 2005 Elsevier B.V. All rights reserved.
doi:10.1016/j.jpowsour.2005.11.035

Nomenclature

C	oxygen concentration in cathode active layer (mol m^{-3})
C_{dl}	double layer capacity (F)
D	diffusion coefficient (m^2 s^{-1})
F	Faraday constant (A s mol^{-1})
j	imaginary number
n	number of electrons
Q	parameter of the CPE (S s$^{\alpha}$)
R	perfect gas constant (J mol^{-1} K^{-1})
R_d	diffusion related resistance (Ω)
R_m	membrane resistance (Ω)
R_p	polarisation resistance (Ω)
S	active area (m^2)
T	temperature (K)
Z	fuel cell's impedance (Ω)
Z_δ	diffusion impedance (Ω)

Greek letters

α	power of the CPE
δ	diffusion layer width (m)
τ_d	diffusion related time constant (s)
ω	pulsation (rad s^{-1})

Softer methods were thus also developed, which focus on the monitoring of data closely related to the state of hydration of the membrane electrode assembly. Pressure drop across the cathode compartment [6,7], as well as current/voltage characteristics [8] were for instance studied. These methods make use of sensors already available on the fuel cell system, and rely on signal processing to monitor the SOH. Voltage measurement is one of the most interesting method as it appears to be the only variable allowing a measurement at the cell level while still being non-intrusive. In [8], the diagnosis solely depends on the processing of steady-state current/voltage data. This proves to be efficient as far as fault detection is concerned, but leads to an indetermination when it comes to fault isolation since flooding and drying out both cause a voltage drop. To overcome this problem, the decision stage of the algorithm makes use of the first derivative of a voltage related fault indicator, assuming that the dynamic behavior of this indicator over the time period during which the failure occurred is always sufficiently different between flooding and drying out. Thus, when considering a fuel cell in a given state with no available history, fault isolation is impossible.

Electrochemical impedance spectroscopy (EIS) has already proved to be a powerful tool to study fuel cell's anode poisoning by CO [9], or to gain insight into the membrane thickness or Nafion loading influence on the fuel cell's performance [10]. Both flooding of the fuel cell and drying out of the membrane were also previously studied in [11]. In [11], a fuzzy logic model, operating on the amplitude and phase of the impedance, is used to monitor the SOH of the fuel cell. EIS measurements taken at open circuit voltage and 10 mA dc current are used. Fault are triggered off-line by either injecting liquid water inside the gas channels or passing heated air through both anode and cathode compartment.

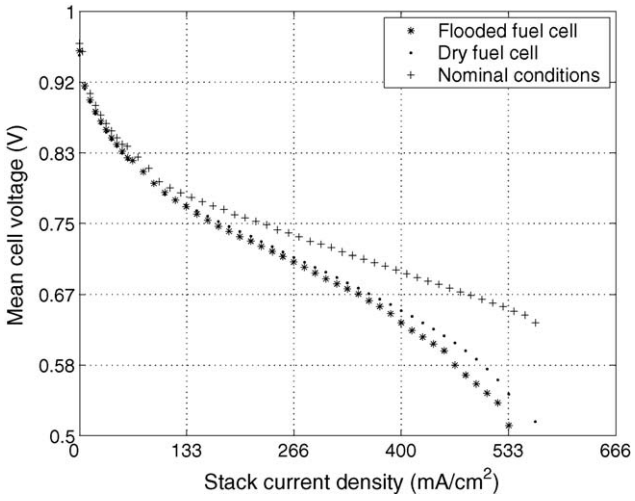

Fig. 1. Measured polarisation curves for a fuel cell working under flooded, dry and nominal conditions.

The study presented in this article focuses on the problem of on-line monitoring of the water content of PEM fuel cells through voltage and current measurements under dynamic conditions. We shall see that dynamic measurements are a way to overcome the indetermination encountered in [8] when it comes to isolating the fault from polarisation curves. As a first step towards on-line fuel cell SOH monitoring, this article shows how a model-based approach coupled with electrochemical impedance spectroscopy measurements could help identify a set of parameters exhibiting a much greater sensitivity and selectivity to flooding and drying than the voltage does.

This article is organized as follows: Section 1.2 presents three examples illustrating the challenges of isolation and early detection of flooding and drying out, as well as the complex link between the inlet gases relative humidity and the fuel cell's state of hydration. The experimental setup used in this study is then briefly presented in Section 2. Section 3 deals with the selection and validation of a simple yet accurate model of the fuel cell's impedance. Finally, Section 4 presents a method to detect and isolate flooding and drying out of the fuel cell based on the monitoring of the model's parameters.

1.2. Scope of the study

To illustrate the indetermination arising from the processing of static measurements, polarisation curves were recorded while the fuel cell was working under nominal, flooded and dried conditions. Fig. 1 shows that for currents above 200 mA cm^{-2}, a faulty fuel cell operates at a significantly lower voltage than a healthy one. However, it seems almost impossible to tell which of the two failures caused the voltage drop: for a given current, excessive drying or flooding of the fuel cell can lead to the same voltage, as seen in Fig. 1, where the "flooded" and "dry" polarisation curves are almost superimposed.

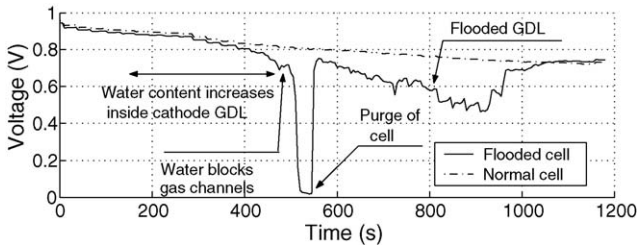

Fig. 2. Flooding of a fuel cell at constant pressure, temperature and stoichiometries, with fully humidified reactants and a slowly increasing current.

Fig. 2 compares the behavior of both a flooded and normal cell as a function of time while current drawn from the stack progressively rises. As can be seen, flooding a fuel cell is a two-step process. The first stage of the process causes a slow voltage drop, as if the current was limited by the diffusion of reactants. This voltage drop is interpreted as being the result of an accumulation of liquid water inside the cathode gas diffusion layer (GDL). The water build-up inside the cathode GDL is a slow process. It can take several minutes before the water actually blocks gas channels. On the contrary, the second stage is a matter of seconds. Once water droplets form inside gas channels, they prevent oxygen from reaching the catalytic sites, thus rapidly driving the cell potential to zero (Fig. 2). Prolonged operation in reactants starved conditions being extremely harmful to the fuel cell [2], the challenge is to detect the flooding while still in stage one, so as to engage corrective action before the cell's voltage drops to zero. This task could be achieved by monitoring each and every cell voltage, but since stacks for transportation application usually count a few hundred cells, this solution is not practical at all. Fig. 2 also demonstrates that flooding does not necessarily occurs at high current density. At the end of the experiment ($t \geq 1000$ s), when the current is the highest, both the once flooded cell and the normal one perform equally well.

Fig. 3 shows the mean cell voltage of the stack during a five-hour long experiment in which the stack was successively operated in flooded, nominal and dry conditions. The dc current was kept constant for the whole duration of the test, so as to ensure that the state of health of the fuel cell is solely responsible for the voltage variation. Cathode inlet gas relative humidity was kept below 50% at all time so as to avoid the flooding of gas distribution channels. As can be seen, there is no obvious way to diagnose the state of health of the stack from the knowledge of its voltage. For a given current, Fig. 3 confirms what had been anticipated from the reading of the polarisation curves of Fig. 1: flooded and dry conditions can lead to the same voltage drop. Moreover, it appears that there is no straightforward link between the inlet gases relative humidity and the state of health of the fuel cell. As the cathode inlet relative humidity gradually decreases between 1500 and 9500 s, the fuel cell undergoes a brutal transition from flooded to nominal state. This transition has been shown to be easily triggered by small twitches in cathode's pressure or gas flow rate once a low enough inlet relative humidity is reached. Thus, it appears that even at humidity level as low as 30%, an unstable equilibrium exists between the GDL and the distribution channels in which the GDL keeps the extra amount of water that has accumulated at high relative humidity

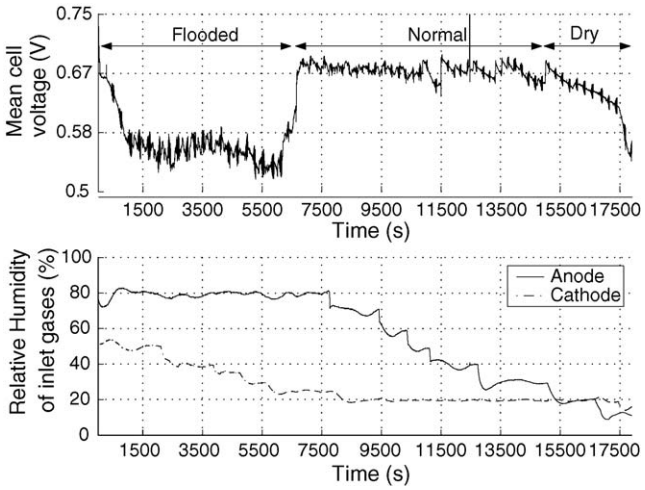

Fig. 3. Mean cell voltage of a fuel cell in flooded, normal and dry condition, as a function of time and relative humidity of inlet gases, with constant pressure, temperature, stoichiometries and current.

level, making it highly hazardous to rely on the inlet relative humidity level to estimate the state of hydration of the membrane electrode assembly.

2. Experimental setup

All measurements were carried out on a stack fed with air and pure hydrogen. So as to ensure stability and homogeneity of the fuel cell under test, active areas below 5 cm^2 [12,13], or single cells [14] are usually chosen for ac impedance measurements. To the knowledge of the authors, the largest active area investigated by means of electrochemical impedance spectroscopy and published to date is 50 cm^2 [15]. In an attempt to come one step closer to a full size stack, a six-cell assembly with an active area of 150 cm^2 was selected for this study. Impedance spectra were computed based on the stack voltage. It introduced a fair amount of inhomogeneity and instability in the system, which, in turn, showed the robustness of the approach. Both flooding and drying out were triggered on-line, by changing the inlet gas relative humidity.

Fuel cell's operating conditions were monitored and controlled through a Greenlight Power FCATS-L test station. Impedance spectra were recorded with a Gamry FC350 connected to a RBL232 50-400-2000 loadbox from TDI Dynaload. The fuel cell was directly connected to the load. Therefore, the anode acts as the reference electrode. ac perturbation was chosen as a function of the direct current drawn, so as to ensure the linear behavior of the fuel cell while compensating for measurement noise and voltage instability of the stack. It ranges from 2 A root mean square (r.m.s.) for a direct current of 80 to 0.1 A r.m.s. for a direct current of 2A. Frequencies ranging from 0.1 Hz to 1 kHz, with 10 measurement points per decade, were used for all of the spectra presented here. Inductive behavior from the wires was predominant above 1 kHz, while instability of the system led to highly unreproducible results below 0.1 Hz.

A full frequency sweep in accuracy mode takes around 5 min to complete. Often, the state of the fuel cell changes between

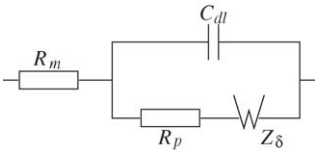

Fig. 4. Randles cell.

the beginning and the end of the impedance measurement, as we shall see in Section 4.1.1, and thus, the assumption of stability, which is essential to the very definition of an impedance, is violated. However, no system fulfills the stability requirement in the theoretical sense, and the challenge is thus to keep the amount of inconsistency introduced by the unavoidable instability to a "reasonable" level. The approaches for ascertaining the degree of consistency include direct integration of the Kramers–Kronig relations, experimental replication of data and regression of electrical circuit analogues to the data [16]. The last two were used in this study. Over 150 impedance spectra were recorded in the course of this study, some experiments being duplicated as many as 10 times. Electrical models made of linear, causal and passive elements were then fitted to the data. These models, which satisfy the Kramers–Kronig relations were found a posteriori to be good and robust fit to the recorded spectra. For instance, regression of our model to a set of spectra recorded at constant time intervals on a fuel cell running in steady state over a period of a few hours led to parameters exhibiting less than 8% of relative variation, much of which aroused in the low frequency part of the spectra. In the high frequency part of the spectra, measurements were found to be reproducible with less than 3% of relative variation. Experimental data were thus deemed consistent. As a corollary, a change in any of the model parameters will be deemed meaningful above a 10% relative variation. Below that threshold, measurement noise and system instability are probably predominant.

3. Fuel cell's impedance model

3.1. Randles cell with Warburg finite-length diffusion element

3.1.1. Theoretical expression

The Randles cell (Fig. 4), is a common and practical way of modeling an electrochemical cell as an equivalent circuit. It consists of four elements: two resistors, R_m, standing for the ohmic resistance of the electrolyte, here the proton exchange membrane, and R_p standing for the polarisation resistance, due to the oxygen reduction reaction; a plane capacitor, C_{dl}, representing the double layer capacitance at the electrode/electrolyte interface; and a Warburg diffusion element.

From the Butler–Volmer equation and Fick's second law of diffusion, it is possible to derive the general expression of the diffusion impedance for a finite length diffusion layer, Z_δ [17]:

$$Z_\delta = \frac{RT}{n^2F^2S\sqrt{j\omega}}\frac{\tanh\sqrt{(j\omega/D)}\delta}{C\sqrt{D}} \tag{1}$$

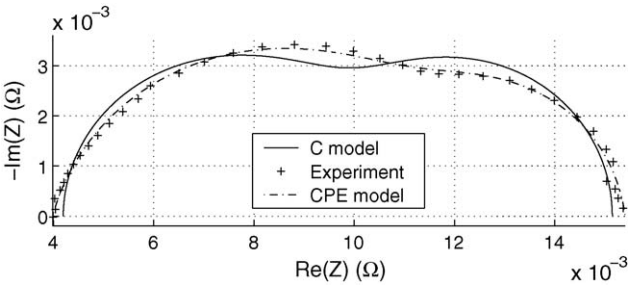

Fig. 5. Comparison between experimental impedance data, a Randles cell model and a Randles cell model with a CPE.

Relation (1) can be re-written as:

$$Z_\delta = \frac{RT}{n^2F^2S\sqrt{j\omega}}\frac{1}{C}\frac{1}{D}\delta\frac{\tanh\sqrt{j\omega(\delta^2/D)}}{\sqrt{\delta^2/D}} \tag{2}$$

which leads to the definition of two parameters, a time constant τ_d,

$$\tau_d = \frac{\delta^2}{D} \tag{3}$$

and a resistance, R_d,

$$R_d = \frac{RT\delta}{n^2F^2SCD} \tag{4}$$

One can check that if all parameters in Eqs. (3) and (4) are expressed in terms of standard units (see Nomenclature), τ_d is dimensionally homogenous to a time (s) and R_d is dimensionally homogenous to an electrical resistance (Ω). This leads to the final expression of the concentration–diffusion impedance:

$$Z_\delta = R_d\frac{\tanh\sqrt{\tau_d j\omega}}{\sqrt{\tau_d j\omega}} \tag{5}$$

Eq. (5) will be used to fit the low frequency part of the impedance spectrum. Relations (3) and (4) will be used to interpret the effects of flooding and drying out at the membrane electrode assembly level, based on the deviation of the parameters with respect to their nominal values.

By further making the assumption that the rate limiting reaction is the oxygen reduction at the cathode, we will neglect the contribution of the anode impedance to the cell impedance. Thus, the equivalent circuit retained to model our fuel cell is that of Fig. 4, and the overall impedance is:

$$Z = R_m + \frac{1}{j\omega C_{dl} + (1/(R_p + Z_\delta))} \tag{6}$$

3.1.2. Fitting the original Randles circuit

As seen in Fig. 5, the fitting of a Randles cell to the experimental data is good but not entirely satisfactory. The bulk of the problem comes from the high-frequency part of the model, for which the Randles cell predicts a semicircle centred on the *x*-axis, while experimental data clearly show a depressed semicircle (i.e. centred below the *x*-axis). As a side-effect, the model misplaces the transition between the two semicircles. This problem is dealt with in the next section.

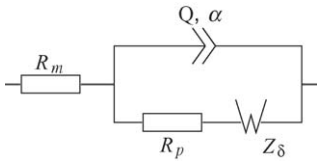

Fig. 6. Randles cell with CPE.

3.2. Adding a Constant Phase Element (CPE)

3.2.1. Theoretical expression

The problem of a high frequency depressed semicircle is commonly encountered when it comes to fitting a model to EIS spectra. These depressed semicircles have been explained by a number of phenomena, depending on the nature of the system being investigated, as for instance in-homogeneous electrode surface [18] or distribution of activation or relaxation processes [19]. However, the common thread among these explanations is that some property of the system is not homogeneous or that there is a distribution of the value of some physical parameter.

These depressed semicircles are usually dealt with by changing the standard plane capacitor of the Randles circuit into a constant phase element (CPE), as seen in Fig. 6. Whereas the standard plane capacitor exhibits a first-order behavior, the CPE impedance is defined by

$$Z_{\mathrm{CPE}} = \frac{1}{Q(j\omega)^{\alpha}} \tag{7}$$

with a value of α usually ranging between 0.5 and 1. While identifying precisely the physical reason behind this non-integer behavior of the fuel cell is out of the scope of this study, it is important to make sure that the use of a CPE is based on some physical properties. Therefore, if the CPE behavior is indeed due to some physical properties of the membrane electrode assembly, the parameter α should remain somewhat constant for a wide range of operating conditions. Otherwise, the introduction of the α parameter would only serve as an extra degree-of-freedom, used by the fitting algorithm to compensate for an inaccurate model.

Over the course of the study presented in this article, some 164 impedance spectra were recorded, in various operating conditions, as depicted in Table 1. For each spectrum, a model was fitted to the data using the ZView software from Scribner Associates Inc. Statistics of the parameter α of Eq. (7) were then studied. The Kolmogorov–Smirnov test was first applied, and it showed that the set of value of α falls within 5% of a normal distribution. A normal probability distribution function was thus fitted to the set, which led to the following parameters:

- mean value: $\overline{\alpha} = 0.8027$,
- 95% confidence interval: $0.7999 \leq \overline{\alpha} \leq 0.8055$,
- standard deviation: $\sigma(\alpha) = 0.0181$.

Considering the compactness of the distribution of the value of α with respect to the rather broad range of operating conditions that were used (see Table 1), it seems reasonable to assume that the value of $\alpha \approx 0.8$ is a constant of our fuel cell and has a physical meaning. As a consequence, the models presented in Section 4 were fitted with a fixed value of $\alpha = 0.8$.

Another problem arising from the use of a CPE instead of a parallel plate condenser is that the parameter Q of Eq. (7) does not have the dimension of a capacitance anymore. While this might be a serious drawback in modeling or sizing studies, it is of less importance here since we are more interested in relative variations of parameters, as a function of the fuel cell's SOH, than in their absolute values. Thus, the impedance of the equivalent circuit is now:

$$Z' = R_{\mathrm{m}} + \frac{1}{(j\omega)^{\alpha} Q + (1/(R_{\mathrm{p}} + Z_{\delta}))} \tag{8}$$

3.2.2. Fitting the modified Randles circuit

The model of the fuel cell's impedance given by Eq. (8), which retains a strong physical meaning and yet a simple structure as well as a small number of parameters, was found to fit very well to our experimental data. A graphical reading of Fig. 5 shows the good agreement between model and experiments. The quality of the fit was estimated from relative errors on the modulus and phase of the impedance. Errors for the spectra in Fig. 5 were found to be below 2% in amplitude and 6% in phase over the whole range of frequency. Both of these values fall below the measurement uncertainty threshold that was defined in Section 2, making it useless to try to further refine the model.

4. Fuel cell's state-of-health monitoring

The three spectra in Fig. 7 were recorded at 70 A dc prior to the recording of the polarisation curves shown in Fig. 1. As opposed to the polarisation curves, each impedance spectrum exhibits its very own set of features. For nominal conditions, one recognises an almost full depressed semicircle in high frequency followed by a smaller semicircle (in fact one fourth of a lemniscate) in low frequency. In the case of a flooded fuel cell, both real and imaginary parts of the impedance grow larger, and the two semicircles are no longer visually resolvable. With a dry fuel cell, the whole spectra is shifted toward the positive side of the real axis. Both semicircles are of comparable size.

4.1. Fault detection

4.1.1. Flooded gas diffusion layer

During this experiment, the relative humidity of inlet gases were held constant at a value of 50% on cathode side and 70% on anode side. The temperature was maintained at 60 °C, a constant

Table 1
Range of operating conditions for which EIS spectra were recorded

Parameter	Min. value	Max. value
Current (A)	40	80
Fuel stoi.	1.2	2
Oxidant stoi.	3	5
Anode RH (%sat.)	10	100
Cathode RH (%sat.)	15	100
Anode pressure (bara)	1	1.5
Cathode pressure (bara)	1	1.5

Table 2
Evolution of the model parameters and cell voltage during the flooding of the GDL

	R_m	Q	R_p	R_d	τ_d	U
Exp1	0.00398	1.109	0.0080	0.0034	0.0872	4.18
Exp3	0.00406	1.080	0.0123	0.0094	0.0818	3.75
Exp5	0.00400	1.102	0.0147	0.0172	0.0784	3.55
Exp12	0.00416	0.936	0.0163	0.0312	0.0947	3.30
Δ_{tot} (%)	+4.6	−15.6	+104	+817	+8.07	−21

Table 3
Evolution of the model parameters and cell voltage while the membrane was getting dry

	R_m	Q	R_p	R_d	τ_d	U
Exp1	0.00512	0.952	0.0099	0.0051	0.1155	4.06
Exp7	0.00685	0.684	0.0108	0.0056	0.1223	3.85
Exp12	0.00880	0.620	0.0130	0.0101	0.1835	3.35
Δ_{tot} (%)	+73	−35	+31	+98	+59	−17

direct current of 70 A was drawn, and the fuel cell stack was operated at atmospheric pressure on both sides. A stoichiometry of 4 was imposed at the cathode, so as to avoid the blocking of gas channels by water droplets. Anode stoichiometry was 1.2. These operating conditions were found to cause a slow flooding of the GDL, steadying at a voltage approximately 20% lower than the nominal voltage, as shown in Fig. 8. The average standard deviation between cell voltages was below 0.05 V. The duration of the experiment was 4000 s, during which impedance spectra were recorded every 300 s using a 2 A r.m.s. ac ripple. They can be seen on the time dependence plot of the mean cell voltage of Fig. 8.

Out of the 13 spectra of Fig. 8, the first, third, fifth and twelfth are plotted in the complex plane in Fig. 9, so as to show the evolution of the impedance as water builds up inside the GDL. The experimental data is represented by symbols and the solid lines represent the simulated curves after fitting the parameters of the equivalent circuit of Fig. 6 to experimental data. It appears clearly that the process of flooding is characterised by the modification of the low frequency part of the fuel cell stack's

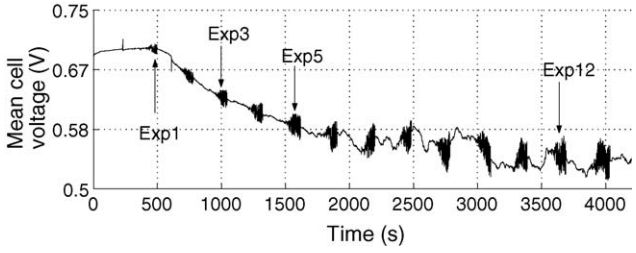

Fig. 8. Mean cell voltage evolution as a function of time while water builds up inside the cathode GDL, at a constant current of 70 A.

impedance, which, in turn, is associated with the diffusion process.

Parameters of the model of Fig. 6 fitted to Exp1, 3, 5 and 12 are given in Table 2. Two parameters in particular are affected by the flooding: R_p and R_d. While the mean cell voltage drops of only 21%, R_p doubles and R_d is multiplied by more than 9, which is well above the 10% uncertainty threshold that was chosen in Section 2. This is a very interesting feature when it comes to the diagnosis of large stacks in which only a few cells become faulty. It is almost impossible to detect a 20%

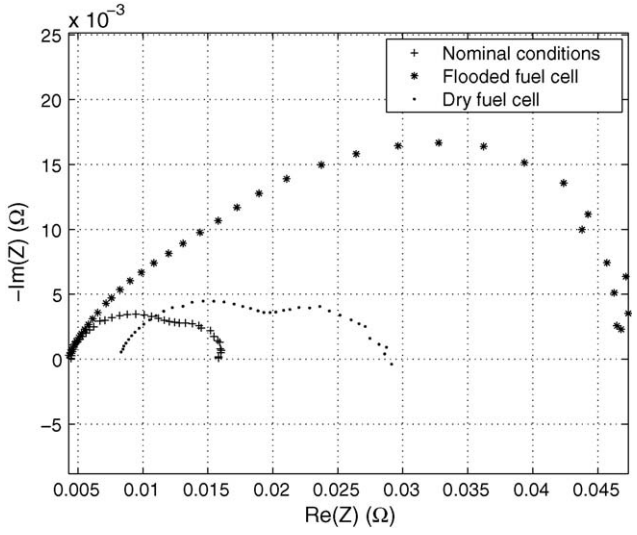

Fig. 7. Nyquist plot of the fuel cell impedance spectra prior to the recording of the polarisation curves of Fig. 1.

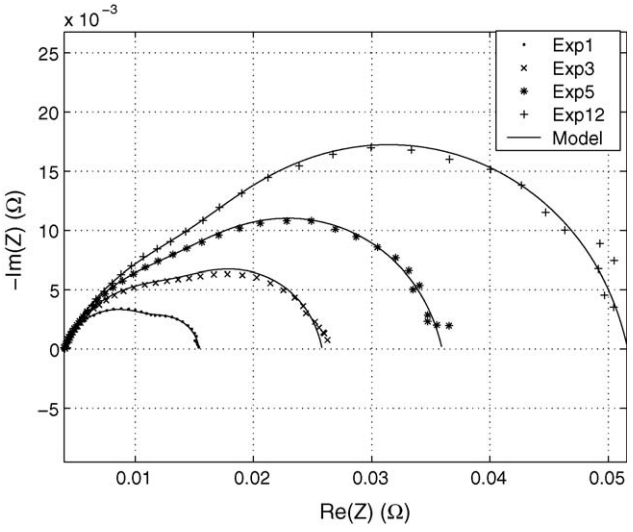

Fig. 9. Nyquist plot of the flooded fuel cell impedance spectra.

voltage drop among tens of healthy cells: the variation will most probably be lost in measurement noise. On the other hand, an almost 10-fold increase of R_d is more likely to be noticeable.

The parameter dependence of R_d is given by Eq. (4). In this relation, some parameters are constants, as for example R, the perfect gas constant, F, the Faraday's constant, n, the number of electrons involved in the reaction, and δ, the width of the diffusion layer. Others can be assumed constant since they are carefully monitored and controlled. This is the case of T, the temperature, and C, the oxygen's concentration, although that last assumption needs a little discussion. The C in Eq. (1) refers to the interfacial concentration of reactant where the reaction takes place. Let us assume that this concentration is directly related to the oxygen partial pressure within the gas distribution channels. Since total pressure, current and air stoichiometry are held constant, there is no reason for the oxygen partial pressure to change during the experiment. Consequently, a change in C could only be explained by a modification of the diffusion phenomena. For instance, several diffusion processes co-exist within the membrane electrode assembly, among which diffusion of oxygen through the GDL, then through the water film and the electrolyte film covering the catalyst agglomerate. Diffusion of protons through the membrane might also be worth considering [20,21]. It is still unclear which one of these steps is the limiting one, much less whether or not the limiting step depends upon the fuel cell's state of health. In the case of flooding, τ_d barely changes during the experiment: +8.07% is not seen as a significant variation with regard to what was said in Section 2, and especially as drying out of the fuel cell yielded a 59% increase of that same parameter (see Table 3). According to Eq. (3), the fact that τ_d did not change means that neither D nor δ did change. Thus, if D, the diffusion coefficient, did not change, it seems safe to assume that the diffusion limiting step did not change during flooding.

R, T, δ, n, F, C and D being constant under the aforementioned assumption, the increase of R_d could be explain by a decrease of S, the active area of the cell. Since the fuel cell is operated in galvanostatic mode, the fraction of the active area which is still available has to deliver a substantially higher current density than in the nominal conditions, which could explain the voltage drop. This explanation is qualitative at best. Our model, with five parameters, cannot possibly capture the complex behavior of water within the membrane electrode assembly. As a hint for further studies, let's remember that a complete blocking of a portion of the active area seems more likely than an increase of the diffusion resistance, which should have shown up in τ_d.

4.1.2. Dried proton exchange membrane

As opposed to what we have seen in Section 4.1.1, a lack of water in the inlet gas can lead to the drying out of the membrane. This fault was triggered by progressively lowering the inlet gas relative humidity to 10% on anode side and 15% on cathode side. The temperature was maintained at 60 °C, a constant direct current of 70 A was drawn, and the fuel cell stack was operated at atmospheric pressure on both sides. Stoichiometries were kept at 1.2 on anode side and 4 on cathode side. As seen in Fig. 10, this

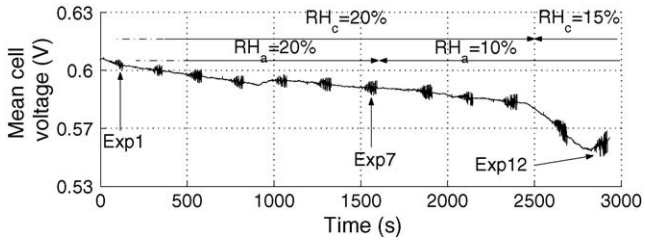

Fig. 10. Mean cell voltage evolution as a function of time while membrane is drying, at a constant current of 70 A.

causes a voltage drop very similar to the one caused by flooding, steadying slightly below 0.57 V per cell.

Out of the 12 spectra of Fig. 10, the first, seventh and twelfth are plotted in the complex plane in Fig. 11, so as to show the evolution of the impedance as the proton exchange membrane dries out. Again, the experimental data is represented by symbols and the solid lines represent the modeled curves after fitting the parameters of the equivalent circuit of Fig. 6 to experimental data. In the case of a drying membrane, the impedance spectra progressively shifts towards the positive part of the real axis, while the low frequency loop grows to a comparable size as the high frequency one.

As shown in Table 3, the variation of the model parameters while the membrane is drying is less dramatic than in the case of flooding. However, the model parameters' sensitivity to the failure is still much higher than the voltages'. At high frequencies, the CPE short-circuits the polarisation resistance and the Warburg impedance, leaving only the membrane resistance in the equivalent circuit. Thus, Fig. 11 confirms that the less water in the membrane, the higher the resistance. It is of interest to note that τ_d is affected by the lack of water, while it was shown in Section 4.1.1 to be robust to its excess. As stated above, this could be explained by either a change in δ, the length of the diffusion layer, or D, the diffusion coefficient. In other words, the diffusion limiting step is likely to have changed, though it is difficult to be more specific.

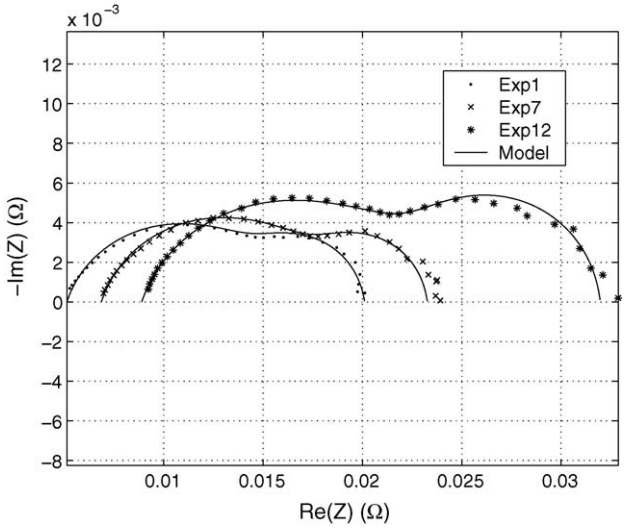

Fig. 11. Nyquist plot of the drying fuel cell impedance spectra.

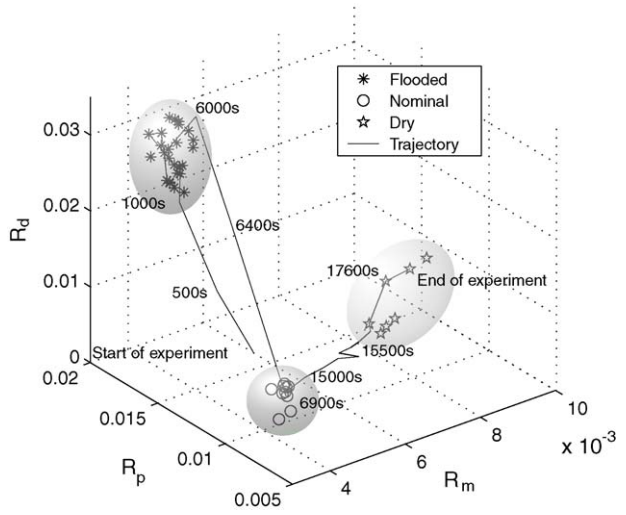

Fig. 12. Evolution of the fuel cell state of health as a function of time.

4.2. Fault isolation

The above sections showed that both flooding of the cathode GDL and drying of the membrane could be efficiently detected via EIS measurements. From the fitting of a Randles circuit, augmented with a CPE, to experimental data, it was found that three parameters were particularly sensitive to the fuel cell stack's state of health. These parameters are the three resistances of the equivalent circuit of Fig. 6: R_m, the membrane resistance, R_p, the polarisation resistance, and R_d, the diffusion resistance. They define a 3D space that can be used to estimate the state of health of the stack.

In Fig. 12, symbols represent triplets (R_m, R_p, R_d) fitted to experimental data. These sets of triplets were used to define parameter subspaces in which the fuel cell state of health is known. For instance, Exp1 of Fig. 10 and Exp1 of Fig. 8 were used, among others, to define the "nominal" subspace of Fig. 12. Exp12 of Fig. 10 is part of the "dry" subspace, and Exp12 of Fig. 8 is part of the "flooded" subspace. Shaded volumes were arbitrary drawn around the data points so as to form three subspaces. It appears in Fig. 12 that each subspace is sufficiently distant from the two others to easily build a decision making algorithm that produces a reliable diagnosis of the fuel cell's SOH.

The results shown in Fig. 3 will now be used to evaluate our method. During the course of this experiment, impedance spectra were regularly recorded. Following the method proposed in this article, parameters of the model of Fig. 6 were fitted to the spectra. For each spectrum, the triplet (R_m, R_p, R_d) was plotted as a solid line in Fig. 12. Thus, the solid line in Fig. 12 represents the evolution of the fuel cell state of health. It can be used as a much more efficient SOH indicator than the mean cell voltage.

At 1000 s, one can see that the fuel cell stack enters the top left subspace, which, in turn, means it starts being flooded. The fuel cell remains flooded for some 4000 s, at which point it quickly returns to the bottom left subspace: normal operation. Low anode inlet gas relative humidity causes the membrane to dry out. At 15 000 s, the fuel cell leaves the "normal operation" subspace, moving toward the bottom right one, which it reaches at 15 500 s. The stack then remains in dry operation mode until the end of the experiment.

5. Conclusion

The Randles model augmented with a CPE was found to be an accurate model of the fuel cell's electrical response over a wide range of operating conditions. The model based approach allowed us to identify a set of three parameters exhibiting high sensitivity to either flooding or drying out of the membrane electrode assembly. Robust and reliable PEM fuel cell's state of hydration monitoring was demonstrated using R_m, the membrane resistance, R_p, the polarisation resistance, and R_d, the diffusion resistance.

Qualitative physical explanations of the variations of the model parameters were proposed. Further and lower level studies and experiments are needed in order to confirm them.

Finally, as the use of an ac spectrometer is not a very convenient solution for on-board integration, work is under way to assess the potential of the FT-EIS concept [22], which makes use of random excitation signals, as possibly those readily available in the fuel cell power plant, for on-line identification of the system's impedance.

Acknowledgements

This work is funded under a "CIFRE" contract conceded by ANRT, with LAGIS Ecole Centrale Lille and PSA Peugeot Citroën. The use of company facilities at PSA Peugeot Citroën as well as the ability to publish this work are gratefully acknowledged.

References

[1] R. Eckl, W. Zehtner, C. Leu, U. Wagner, Experimental analysis of water management in self-humidifying polymer electrolyte fuel cell stack, J. Power Sources 138 (2004) 137–144.
[2] S.D. Knights, K.M. Colbow, J. St-Pierre, D.P. Wilkinson, Aging mechanisms and lifetime of PEFC and DMFC, J. Power Sources 127 (2004) 127–134.
[3] K. Tüber, D. Pózca, C. Hebling, Visualisation of water build up in the cathode of a transparent PEM fuel cell, J. Power Sources 124 (2) (2003) 403–414.
[4] M. Mench, Q. Dong, C. Wang, In situ water distribution measurements in a polymer electrolyte fuel cell, J. Power Sources 124 (1) (2003) 90–98.
[5] A. Tsukada, E. Lehmann, P. Vontobel, G. Scherer, In situ observation of water condensation in an operating polymer electrolyte fuel cell by means of neutron imaging at the spallation neutron source (SINQ), Tech Report Paul Scherrer Inst. 5 (1999) 84.
[6] W. He, G. Lin, T.V. Nguyen, Diagnostic tool to detect electrode flooding in proton exchange membrane fuel cells, AIChE J. 49 (12) (2003) 3221.
[7] A.D. Bosco, M.H. Fronk, Fuel cell flooding detection and correction, US Patent 6,103,409 (2000).
[8] D. Hissel, M.C. Péra, J.M. Kauffmann, Diagnosis of automotive fuel cell power generators, J. Power Sources 128 (2) (2004) 239–246.
[9] N. Wagner, M. Schultze, Change of electrochemical impedance spectra during CO poisoning of the Pt and Pt–Ru anodes in a membrane fuel cell (PEFC), Electrochim. Acta 48 (2003) 3899–3907.

[10] Q. Guo, M. Cayetano, Y. Tsou, E.S. De Castro, R.E. White, Study of ionic conductivity profiles of the air cathode of a pemfc by ac impedance spectroscopy, J. Electrochem. Soc. 150 (11) (2003) A1440–A1449.
[11] C. Fennie, D. Reisner, J. Barbetta, P. Singh, Fuzzy logic-based state-of-health determination of PEM fuel cells, Proceedings of the EVS18, Berlin, 2001.
[12] V.A. Paganin, C.L.F. Oliveira, E.A. Ticianelli, T.E. Springer, E.R. Gonzalez, Modelistic interpretation of the impedance response of a polymer electrolyte fuel cell, Electrochim. Acta 43 (1998) 3761–3766.
[13] X. Wang, I.-M. Hsing, Y.-J. Leng, P.-L. Yue, Model interpretation of electrochemical impedance spectroscopy and polarization behavior of H_2/CO mixture oxidation in polymer electrolyte fuel cells, Electrochim. Acta 46 (2001) 4397–4405.
[14] T. Abe, H. Shima, K. Watanabe, Y. Ito, Study of PEFCs by ac impedance, current interrupt, and dew point measurements. I. Effect of humidity in oxygen gas, J. Electrochem. Soc. 151 (1) (2004) A101–A105.
[15] R. Makharia, M.F. Mathias, D.R. Baker, Measurement of catalyst layer electrolyte resistance in PEFCs using electrochemical impedance spectroscopy, J. Electrochem. Soc. 152 (5) (2005) A970–A977.
[16] P. Agarwal, M.E. Orazem, L.H. Garcia-Rubio, Application of measurement models to impedance spectroscopy, J. Electrochem. Soc. 142 (12) (1995) 4159–4168.
[17] H.H. Girault, Electrochimie physique et analytique, Presses polytechniques et universitaires romandes, 2001.
[18] C.H. Kim, S.I. Pyun, J.H. Kim, An investigation of the capacitance dispersion on the fractal carbon electrode with edge and basal orientations, Electrochim. Acta 48 (2003) 3455.
[19] M.E. Orazem, P. Shukla, M.A. Membrino, Extension of the measurement model approach for deconvultion of underlying distributions for impedance measurements, Electrochim. Acta 47 (2002) 2027–2034.
[20] F. Jaouen, G. Lindbergh, G. Sundholm, Investigation of mass-transport limitations in the solid polymer fuel cell cathode. i. Mathematical model, J. Electrochem. Soc. 149 (4) (2002) A437–A447.
[21] J. Ihonen, F. Jaouen, G. Lindbergh, A. Lundblad, G. Sundholm, Investigation of mass-transport limitations in the solid polymer fuel cell cathode. ii. Experimental, J. Electrochem. Soc. 149 (4) (2002) A448–A454.
[22] J.E. Garland, C.M. Petit, D. Roy, Analysis of experimental constraints and variables for time resolved detection of Fourier transform electrochemical impedance spectra, Electrochim. Acta 49 (2004) 2623.